First search for extremely high energy cosmogenic neutrinos with the IceCube Neutrino Observatory

R. Abbasi,[28] Y. Abdou,[22] T. Abu-Zayyad,[33] J. Adams,[16] J. A. Aguilar,[28] M. Ahlers,[32] K. Andeen,[28] J. Auffenberg,[39] X. Bai,[31] M. Baker,[28] S. W. Barwick,[24] R. Bay,[7] J. L. Bazo Alba,[40] K. Beattie,[8] J. J. Beatty,[18,19] S. Bechet,[13] J. K. Becker,[10] K.-H. Becker,[39] M. L. Benabderrahmane,[40] J. Berdermann,[40] P. Berghaus,[28] D. Berley,[17] E. Bernardini,[40] D. Bertrand,[13] D. Z. Besson,[26] M. Bissok,[1] E. Blaufuss,[17] D. J. Boersma,[1] C. Bohm,[34] S. Böser,[11] O. Botner,[37] L. Bradley,[36] J. Braun,[28] S. Buitink,[8] M. Carson,[22] D. Chirkin,[28] B. Christy,[17] J. Clem,[31] F. Clevermann,[20] S. Cohen,[25] C. Colnard,[23] D. F. Cowen,[36,35] M. V. D'Agostino,[7] M. Danninger,[34] J. C. Davis,[18] C. De Clercq,[14] L. Demirörs,[25] O. Depaepe,[14] F. Descamps,[22] P. Desiati,[28] G. de Vries-Uiterweerd,[22] T. DeYoung,[36] J. C. Díaz-Vélez,[28] J. Dreyer,[10] J. P. Dumm,[28] M. R. Duvoort,[38] R. Ehrlich,[17] J. Eisch,[28] R. W. Ellsworth,[17] O. Engdegård,[37] S. Euler,[1] P. A. Evenson,[31] O. Fadiran,[4] A. R. Fazely,[6] T. Feusels,[22] K. Filimonov,[7] C. Finley,[34] M. M. Foerster,[36] B. D. Fox,[36] A. Franckowiak,[11] R. Franke,[40] T. K. Gaisser,[31] J. Gallagher,[27] R. Ganugapati,[28] M. Geisler,[1] L. Gerhardt,[8,7] L. Gladstone,[28] T. Glüsenkamp,[1] A. Goldschmidt,[8] J. A. Goodman,[17] D. Grant,[21] T. Griesel,[29] A. Groß,[16,23] S. Grullon,[28] M. Gurtner,[39] C. Ha,[36] A. Hallgren,[37] F. Halzen,[28] K. Han,[16] K. Hanson,[28] K. Helbing,[39] P. Herquet,[30] S. Hickford,[16] G. C. Hill,[28] K. D. Hoffman,[17] A. Homeier,[11] K. Hoshina,[28] D. Hubert,[14] W. Huelsnitz,[17] J.-P. Hülß,[1] P. O. Hulth,[34] K. Hultqvist,[34] S. Hussain,[31] R. L. Imlay,[6] A. Ishihara,[15,*] J. Jacobsen,[28] G. S. Japaridze,[4] H. Johansson,[34] J. M. Joseph,[8] K.-H. Kampert,[39] A. Kappes,[28,†] T. Karg,[39] A. Karle,[28] J. L. Kelley,[28] N. Kemming,[9] P. Kenny,[26] J. Kiryluk,[8,7] F. Kislat,[40] S. R. Klein,[8,7] S. Knops,[1] J.-H. Köhne,[20] G. Kohnen,[30] H. Kolanoski,[9] L. Köpke,[29] D. J. Koskinen,[36] M. Kowalski,[11] T. Kowarik,[29] M. Krasberg,[28] T. Krings,[1] G. Kroll,[29] K. Kuehn,[18] T. Kuwabara,[31] M. Labare,[13] S. Lafebre,[36] K. Laihem,[1] H. Landsman,[28] R. Lauer,[40] R. Lehmann,[9] D. Lennarz,[1] J. Lünemann,[29] J. Madsen,[33] P. Majumdar,[40] R. Maruyama,[28] K. Mase,[15,‡] H. S. Matis,[8] M. Matusik,[39] K. Meagher,[17] M. Merck,[28] P. Mészáros,[35,36] T. Meures,[1] E. Middell,[40] N. Milke,[20] J. Miller,[37] T. Montaruli,[28,§] R. Morse,[28] S. M. Movit,[35] R. Nahnhauer,[40] J. W. Nam,[24] U. Naumann,[39] P. Nießen,[31] D. R. Nygren,[8] S. Odrowski,[23] A. Olivas,[17] M. Olivo,[37,10] M. Ono,[15] S. Panknin,[11] L. Paul,[1] C. Pérez de los Heros,[37] J. Petrovic,[13] A. Piegsa,[29] D. Pieloth,[20] R. Porrata,[7] J. Posselt,[39] P. B. Price,[7] M. Prikockis,[36] G. T. Przybylski,[8] K. Rawlins,[3] P. Redl,[17] E. Resconi,[23] W. Rhode,[20] M. Ribordy,[25] A. Rizzo,[14] J. P. Rodrigues,[28] P. Roth,[17] F. Rothmaier,[29] C. Rott,[18] C. Roucelle,[23] T. Ruhe,[20] D. Rutledge,[36] B. Ruzybayev,[31] D. Ryckbosch,[22] H.-G. Sander,[29] S. Sarkar,[32] K. Schatto,[29] S. Schlenstedt,[40] T. Schmidt,[17] D. Schneider,[28] A. Schukraft,[1] A. Schultes,[39] O. Schulz,[23] M. Schunck,[1] D. Seckel,[31] B. Semburg,[39] S. H. Seo,[34] Y. Sestayo,[23] S. Seunarine,[12] A. Silvestri,[24] A. Slipak,[36] G. M. Spiczak,[33] C. Spiering,[40] M. Stamatikos,[18,‖] T. Stanev,[31] G. Stephens,[36] T. Stezelberger,[8] R. G. Stokstad,[8] S. Stoyanov,[31] E. A. Strahler,[14] T. Straszheim,[17] G. W. Sullivan,[17] Q. Swillens,[13] I. Taboada,[5] A. Tamburro,[33] O. Tarasova,[40] A. Tepe,[5] S. Ter-Antonyan,[6] S. Tilav,[31] P. A. Toale,[36] D. Tosi,[40] D. Turčan,[17] N. van Eijndhoven,[14] J. Vandenbroucke,[7] A. Van Overloop,[22] J. van Santen,[9] B. Voigt,[40] C. Walck,[34] T. Waldenmaier,[9] M. Wallraff,[1] M. Walter,[40] C. Wendt,[28] S. Westerhoff,[28] N. Whitehorn,[28] K. Wiebe,[29] C. H. Wiebusch,[1] G. Wikström,[34] D. R. Williams,[2] R. Wischnewski,[40] H. Wissing,[17] K. Woschnagg,[7] C. Xu,[31] X. W. Xu,[6] G. Yodh,[24] S. Yoshida,[15,¶] and P. Zarzhitsky[2]

(IceCube Collaboration)

[1]*III. Physikalisches Institut, RWTH Aachen University, D-52056 Aachen, Germany*
[2]*Department of Physics and Astronomy, University of Alabama, Tuscaloosa, Alabama 35487, USA*
[3]*Department of Physics and Astronomy, University of Alaska Anchorage, 3211 Providence Dr., Anchorage, Alaska 99508, USA*
[4]*CTSPS, Clark-Atlanta University, Atlanta, Georgia 30314, USA*
[5]*School of Physics and Center for Relativistic Astrophysics, Georgia Institute of Technology, Atlanta, Georgia 30332, USA*
[6]*Department of Physics, Southern University, Baton Rouge, Louisiana 70813, USA*
[7]*Department of Physics, University of California, Berkeley, California 94720, USA*
[8]*Lawrence Berkeley National Laboratory, Berkeley, California 94720, USA*
[9]*Institut für Physik, Humboldt-Universität zu Berlin, D-12489 Berlin, Germany*
[10]*Fakultät für Physik and Astronomie, Ruhr-Universität Bochum, D-44780 Bochum, Germany*
[11]*Physikalisches Institut, Universität Bonn, Nussallee 12, D-53115 Bonn, Germany*
[12]*Department of Physics, University of the West Indies, Cave Hill Campus, Bridgetown BB11000, Barbados*
[13]*Université Libre de Bruxelles, Science Faculty CP230, B-1050 Brussels, Belgium*
[14]*Vrije Universiteit Brussel, Dienst ELEM, B-1050 Brussels, Belgium*
[15]*Department of Physics, Chiba University, Chiba 263-8522, Japan*
[16]*Department of Physics and Astronomy, University of Canterbury, Private Bag 4800, Christchurch, New Zealand*

[17]*Department of Physics, University of Maryland, College Park, Maryland 20742, USA*
[18]*Department of Physics and Center for Cosmology and Astro-Particle Physics, Ohio State University, Columbus, Ohio 43210, USA*
[19]*Department of Astronomy, Ohio State University, Columbus, Ohio 43210, USA*
[20]*Department of Physics, TU Dortmund University, D-44221 Dortmund, Germany*
[21]*Department of Physics, University of Alberta, Edmonton, Alberta, Canada T6G 2G7*
[22]*Department of Subatomic and Radiation Physics, University of Gent, B-9000 Gent, Belgium*
[23]*Max-Planck-Institut für Kernphysik, D-69177 Heidelberg, Germany*
[24]*Department of Physics and Astronomy, University of California, Irvine, California 92697, USA*
[25]*Laboratory for High Energy Physics, École Polytechnique Fédérale, CH-1015 Lausanne, Switzerland*
[26]*Department of Physics and Astronomy, University of Kansas, Lawrence, Kansas 66045, USA*
[27]*Department of Astronomy, University of Wisconsin, Madison, Wisconsin 53706, USA*
[28]*Department of Physics, University of Wisconsin, Madison, Wisconsin 53706, USA*
[29]*Institute of Physics, University of Mainz, Staudinger Weg 7, D-55099 Mainz, Germany*
[30]*Université de Mons, 7000 Mons, Belgium*
[31]*Bartol Research Institute and Department of Physics and Astronomy, University of Delaware, Newark, Delaware 19716, USA*
[32]*Department of Physics, University of Oxford, 1 Keble Road, Oxford OX1 3NP, United Kingdom*
[33]*Department of Physics, University of Wisconsin, River Falls, Wisconsin 54022, USA*
[34]*Oskar Klein Centre and Department of Physics, Stockholm University, SE-10691 Stockholm, Sweden*
[35]*Department of Astronomy and Astrophysics, Pennsylvania State University, University Park, Pennsylvania 16802, USA*
[36]*Department of Physics, Pennsylvania State University, University Park, Pennsylvania 16802, USA*
[37]*Department of Physics and Astronomy, Uppsala University, Box 516, S-75120 Uppsala, Sweden*
[38]*Department of Physics and Astronomy, Utrecht University/SRON, NL-3584 CC Utrecht, The Netherlands*
[39]*Department of Physics, University of Wuppertal, D-42119 Wuppertal, Germany*
[40]*DESY, D-15735 Zeuthen, Germany*

(Received 7 July 2010; published 7 October 2010)

We report on the results of the search for extremely-high energy neutrinos with energies above 10^7 GeV obtained with the partially ($\sim 30\%$) constructed IceCube in 2007. From the absence of signal events in the sample of 242.1 days of effective live time, we derive a 90% C.L. model independent differential upper limit based on the number of signal events per energy decade at $E^2\phi_{\nu_e+\nu_\mu+\nu_\tau} \simeq 1.4 \times 10^{-6}$ GeV cm^{-2} sec^{-1} sr^{-1} for neutrinos in the energy range from 3×10^7 to 3×10^9 GeV.

DOI: 10.1103/PhysRevD.82.072003 PACS numbers: 98.70.Sa, 95.85.Ry

I. INTRODUCTION

Detection of extremely-high energy (EHE) neutrinos with energies greater than 10^7 GeV may shed light on the long standing puzzle of the origin of EHE cosmic rays [1,2]. Several observational results have indicated that these EHE cosmic rays (EHECRs) are of extragalactic origin [3]. Further elucidation of their production mechanism by EHECR observation is, however, limited because the collisions of EHECR with the cosmic microwave background photons—known as the Greisen-Zatsepin-Kuzmin (GZK) mechanism [4]—prevent EHECRs from propagating over cosmological distances without losing a sizable fraction of their energy. On the other hand, cosmogenic neutrinos [5] produced by the GZK mechanism via photoproduced π meson decay as $\pi^\pm \rightarrow \mu^\pm \nu_\mu \rightarrow e^\pm \nu_e \nu_\mu$ carry information on the EHECR source evolution and the maximum energy of EHECRs at their production sites [6].

Detection of these EHE neutrinos is an experimental challenge because the very low EHE neutrino fluxes require a very large detector. The large size of the IceCube neutrino observatory [7], currently under construction at the geographic South Pole, will make it more effective than previous experiments in the search for these neutrinos [8,9]. Interactions of ν_μ, ν_e, and ν_τ and their antiparticles are observed through the Cherenkov radiation emitted by secondary particles. In the following, we do not distinguish between ν and $\bar{\nu}$; the simulations and sensitivity calculations assume an equal mixture of particles and antiparticles.

In this paper we will describe the first results of a search for signatures of cosmogenic neutrinos in the 2007 data acquired by the partially constructed IceCube neutrino observatory. This analysis selects events which produce a large amount of light in the detector. Based on simple criteria, such as the total number of observed Cherenkov

*Corresponding author.
aya@hepburn.s.chiba-u.ac.jp
†Also at Universität Erlangen-Nürnberg, Physikalisches Institut, D-91058, Erlangen, Germany.
‡Corresponding author.
mase@hepburn.s.chiba-u.ac.jp
§Also at Università di Bari and Sezione INFN, Dipartimento di Fisica, I-70126, Bari, Italy.
‖Also at NASA Goddard Space Flight Center, Greenbelt, MD 20771, USA.
¶Corresponding author.
syoshida@hepburn.s.chiba-u.ac.jp

photons and the results of reconstruction algorithms, it selects candidate neutrino events. Although ν_μ, ν_e, and ν_τ interactions look very different in IceCube, the selection criteria are sensitive to all three flavors.

II. THE ICECUBE DETECTOR

IceCube is a cubic-kilometer, high-energy cosmic neutrino telescope which is currently under construction. It uses the 2800 m thick glacial ice as a Cherenkov medium. Cherenkov photons emitted by relativistic charged particles, notably muons, electrons, and taus produced in charged current interactions and their secondaries, are detected by an array of photon sensors, known as digital optical modules (DOMs) [10]. The DOMs deep below the ice surface are deployed along electrical cable bundles that carry power and communication between the DOMs and surface electronics. The cable assemblies, often called strings, are lowered into holes drilled to a depth of 2450 m. The DOMs, spaced at intervals of 17 m, occupy the bottom 1000 m of each string. The strings are arranged in a hexagonal lattice pattern with a spacing of approximately 125 m. DOMs are also frozen into tanks located at the surface near the top of each hole. The tanks constitute an air shower array called IceTop [11].

The DOMs enclose a down-looking 25 cm photomultiplier tube (PMT) [12] with data acquisition and calibration electronics, light emitting diodes for calibration, and also data compression, communications, and control hardware [10] in a 35 cm diameter pressure sphere. Almost all of the PMTs are run at a gain of 10^7; PMT saturation effects become important at signal levels of about 5000 photoelectrons in a single DOM in 50 ns. When the DOM detects a photoelectron, it initiates an acquisition cycle, recording the PMT output with two waveform digitizer systems. The first system samples every 3.3 ns for 400 ns, with 14 bits of dynamic range. The second system samples every 25 ns for 6.4 μs, with 10 bits of dynamic range. The data acquisition system is designed such that the first system is sensitive to a bright photon source at close distance and the second system captures signal induced by photons emitted at large distance. This analysis uses the total number of photoelectrons detected by the PMTs as a measure of the event energy. For each DOM, the charge used is the one from whichever system recorded a larger number of photoelectrons. Because of the significant DOM-to-DOM differences in saturation behavior, the current analysis does not attempt to correct for PMT saturation. So, the signals from brightly illuminated DOMs are naturally truncated.

III. DATA AND SIMULATION

This analysis uses data collected from May 2007 through April 2008, when IceCube consisted of 22 strings (IC-22; 1320 DOMs) and 52 IceTop tanks. In order to greatly reduce random noise from radioactivity, in IC22 the DOMs only recorded signal waveforms when a local coincidence condition was satisfied, i.e. when an adjoining or next-to-nearest neighbor DOM was triggered within ± 1 μs. In 2007, the trigger selected time periods when 8 or more DOMs recorded local coincidence signals within 5 μs; when this happened, all hits within a 20 μs window were stored as an event. The average trigger rate was about 550 Hz. The high-multiplicity event sample used in this analysis imposes an additional condition requiring NDOM ≥ 80, where NDOM is the number of hit DOMs in an event. The average high-multiplicity event rate was approximately 1.5 Hz with a seasonal variation of 17%. A total of 3.2×10^7 events were tagged as high-multiplicity during the effective live time of 242.1 days (excluding the periods of unstable operation).

The high-multiplicity cut reduces the data by a factor of $\sim 3 \times 10^{-3}$ while preserving approximately 70% of the GZK neutrinos with projected trajectories that pass within 880 m of the center of IceCube. Here, and below, the GZK signal rates are based on the GZK spectra and flux calculated by Ref. [6] assuming an all-proton composition with a moderately strong source evolution, $(z+1)^m$ with $m = 4$ extending to $z = 4.0$. Neutrino oscillations modify the neutrino flavor ratio over the cosmological distances they travel and the fluxes at the Earth were calculated as in Ref. [13]. Note that the flavor ratio ν_e:ν_μ:ν_τ of cosmogenic neutrinos at the Earth is different from 1:1:1 as primary energy spectra of ν_e and ν_μ produced by the GZK mechanism are different because of a significant contribution of ν_e from neutron decay. This enhancement was included in the GZK neutrino flux calculations used here.

EHE neutrinos were simulated with the JULIET package [9] to generate and propagate the neutrinos through the Earth. All three flavors of neutrinos were simulated with energies between 10^5 and 10^{11} GeV. The resulting secondary muons and taus produced in the neutrino interactions are propagated through the rock and ice near the IceCube volume, also by JULIET. Hadronic and electromagnetic showers are also simulated; all of these showers are treated as point sources, without accounting for the LPM effect. The background muon bundles from cosmic rays in the energy range 10^6 to 10^{10} GeV were generated using CORSIKA [14] version 6.720 with the SIBYLL 2.1 hadronic interaction model or with QGSJET-II, without charm production [15]. The uncertain prompt muon component from charm decay may contribute to the background events [16]. The muons were propagated through the Earth using MMC [17]. Departures of observed data distributions from those of the CORSIKA based background events prompted us to also develop a phenomenological background model based on fits to data. Emission of Cherenkov photons and their propagation in the ice was simulated by the Photonics package [18]. Measurement of the absolute number of Cherenkov photons is important in the EHE neutrino

search as it closely relates to the energy of the high-energy muons, taus, or electrons produced by EHE neutrinos. Therefore, the detection efficiency of the DOMs must be understood with good precision. The primary element, the PMT, is calibrated in the laboratory using a nitrogen laser to measure the photon detection efficiency [12]. This bare PMT data are used in a simulation package which propagates photons inside the glass sphere and the optical gel to the photocathode surface. The DOM simulation is followed by waveform calibration and the trigger condition is included in the simulation chain.

IV. ANALYSIS

A. Extremely-high energy event signatures and the initial event filter

The event signatures from ν_μ, ν_e, and ν_τ are very different. IceCube mainly detects cosmogenic neutrinos by the signals from the secondary muons and taus generated in the neutrino interaction in the rock or ice. At high energies, these particles are seen in the detector as series of energetic cascades from radiative energy loss processes such as pair creation, bremsstrahlung, and photonuclear interactions, rather than minimum-ionizing tracks. The radiative energy losses are approximately proportional to the energy of the muon or the tau, and so is the Cherenkov light yield. Electron neutrinos produce electromagnetic and hadronic showers, which are relatively compact sources of Cherenkov light. Muon and tau neutrinos within IceCube will also produce a hadronic shower from the struck nucleon, in addition to the muon or tau secondary.

Shown in Fig. 1 is the simulated distribution of the total number of photoelectrons per event (NPE) recorded by the the IC-22 detector as a function of the simulated true muon energy. A clear correlation between NPE and the energy of particles measured near IceCube is observed. The energies are sampled at a radius of 880 m from the IceCube center. This definition of energy is labeled ''in-ice energy'' and used throughout this paper. The visible departure from linearity for large NPE stems from the saturation of the detector during signal capture. Approximately 30% of EHE signal events are due to neutrino interactions inside the IceCube detector volume initiating a hadronic or electromagnetic cascade. The correlation between NPE and incoming neutrino energy also holds for these events. Electron neutrinos are detectable via this channel.

Because the energy spectrum of background atmospheric muons (both single muons and bundles) falls steeply with energy, the GZK neutrino flux should dominate over background in the high NPE region. Since the through-going muons and taus induced by EHE neutrinos enter into the IceCube volume mainly horizontally [8,9], the signal search criteria are chosen to favor roughly horizontal high NPE events.

The high-multiplicity NDOM $\geq$ 80 sample is dominated by atmospheric background muons. The next step of the analysis selects events with NPE $> 10^4$. This reduces the background by 3 orders of magnitude, leaving 6528 events, still dominated by background, while the GZK signal reduction is $\sim$24%.

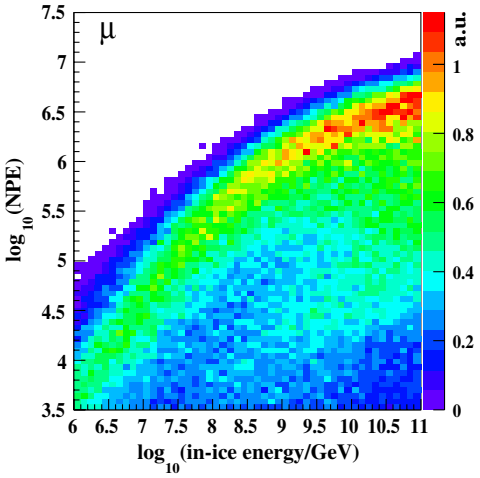

FIG. 1 (color online). Event distribution from Monte Carlo simulations of single muons with the IC-22 detector configurations in a plane of NPE and simulated true energy. The muon energy is given when the muon is 880 meters from the IceCube center (in-ice energy). The 80 DOM multiplicity cut (level-1 cut) is applied. The charged lepton energy distribution is assumed to follow E^{-1} in this plot for illustrative purposes. Only particles with trajectories intersecting within 880 m from the center of IceCube array are considered in the plots. More distant events do not contribute to the data sample.

Table I summarizes the number of events remaining at each level of the initial filtering. In order to estimate the background in the very high-energy region, the simulated data are compared to the experimental data in the region $10^4 <$ NPE $< 10^5$. The present analysis follows the blind analysis technique. In keeping with the IceCube blindness policy, events with NPE $\geq 10^5$ were not used for determining the background or setting cuts. This NPE threshold was chosen so that the possible contribution from signal events in the studied sample was negligible.

B. High-energy muon background

Bundles of muons generated in cosmic-ray air showers are the major background for the EHE neutrino signal search, because multiple muon tracks with a small geometrical separation resemble a single high-energy muon in the IceCube detector. The multiplicity, energy distribution, and separation distances for these muon bundles are not fully understood. Two independent Monte Carlo simulations are carried out to estimate the muon-bundle background in this EHE neutrino signal search.

The first is the full cosmic-ray air shower simulation with light and heavy ion primaries using the CORSIKA (SIBYLL) package [14]. Two extreme cases of composition are used to address the event rate variation due to the

TABLE I. Number of events at different filter levels for 242.1 days in 2007. The simulation predictions for the atmospheric muon background using the CORSIKA-SIBYLL package, the empirical model, and that for the GZK cosmogenic neutrino model are also listed for comparison. Errors shown here are statistical only. Refer to Sec. IVA for the definitions.

Filter levels	Observational data	Empirical model	CORSIKA (iron)	CORSIKA (proton)	Signal (GZK1 [6])
Level 1 (NDOM $\geq$ 80)	3.195×10^7	...	$(1.84 \pm 0.08) \times 10^7$	$(7.71 \pm 0.45) \times 10^6$	$(886 \pm 8.9) \times 10^{-3}$
Level 2 (NPE $> 10^4$)	6528	$(6.82 \pm 0.42) \times 10^3$	$(1.09 \pm 0.09) \times 10^4$	$(1.63 \pm 0.17) \times 10^3$	$(670 \pm 7.5) \times 10^{-3}$

uncertainty in the primary cosmic-ray mass population. While the full air shower simulation includes a calculation of the production spectra of the multiple muons from meson decay, the simulation still introduces a large uncertainty because both the primary composition at relevant cosmic-ray energies ($> 10^7$ GeV) and the hadronic interaction model are highly uncertain.

The second simulation uses a model relying on a phenomenological fit to part of the experimental high-energy data. This empirical model approximates multiple muon tracks in an event by a single high-energy muon which is adequate at very high energies for the variables used in this analysis. The single muon approximation predicts larger fluctuations in NPE due to radiative energy losses of energetic muons, giving a rather conservative estimate of the background passing rate. The two independent sets of simulations with top-down and bottom-up approaches to describe the observational data complement each other improving the reliability of the background estimation.

1. Background estimation with CORSIKA

Figure 2 shows distributions for data and simulations at level-2 for NPE, the reconstructed zenith angle (θ), and the center-of-gravity depth of the events (z_{COG}). The CORSIKA NPE distribution is extrapolated to the higher NPE region. Extrapolation was necessary mainly because of a lack of simulated CORSIKA events at primary cosmic-ray energies above 10^{10} GeV. The extrapolation accounts for the observed GZK cutoff at an energy around 5×10^{19} eV. The NPE-weighted LineFit algorithm was used to reconstruct zenith angle in this initial study. The NPE-weighted LineFit is a simple minimization of $\chi^2 = \Sigma_i NPE_i(\vec{r}_i - \vec{r}_{\mathrm{COG}} - t_i\vec{v})^2$, where t_i and NPE_i represent, respectively, the time of the first photoelectron and the number of photoelectrons recorded by the ith DOM at the position $\vec{r}_i$ and $\vec{r}_{\mathrm{COG}} \equiv (\frac{\Sigma_i \mathrm{NPE}_i x_i}{\Sigma_i \mathrm{NPE}_i}, \frac{\Sigma_i \mathrm{NPE}_i y_i}{\Sigma_i \mathrm{NPE}_i}, \frac{\Sigma_i \mathrm{NPE}_i z_i}{\Sigma_i \mathrm{NPE}_i})$ is the NPE-weighted position of the center of gravity of the hits. The fit ignores the geometry of the Cherenkov cone and the optical properties of the medium and assumes light traveling with a velocity $\vec{v}$ along a one-dimensional path through the detector, passing through the center of gravity.

The measured event rates are close to the simulated rates based on CORSIKA-SIBYLL with iron primaries and above those based on CORSIKA-SIBYLL proton data in most regions. A significant discrepancy can be found in the rate of events with $\cos\theta \leq 0.3$, i.e. events reconstructed as horizontal or up-going, which is largely underestimated. Replacing SIBYLL with other hadronization models (e.g. QGSJET-II) does not change this behavior. The discrepancy may be due to a combination of uncertainties in the hadronic interaction models, cosmic-ray flux, and Cherenkov photon propagation in the glacial ice. Since the horizon is the key region for the EHE neutrino search, the background estimations were supplemented by an empirical model fit to a subsample of the data.

2. Construction of an empirical model

The empirical model is optimized to match the level-2 experimental data ($10^4 < \mathrm{NPE} < 10^5$). The possible signal

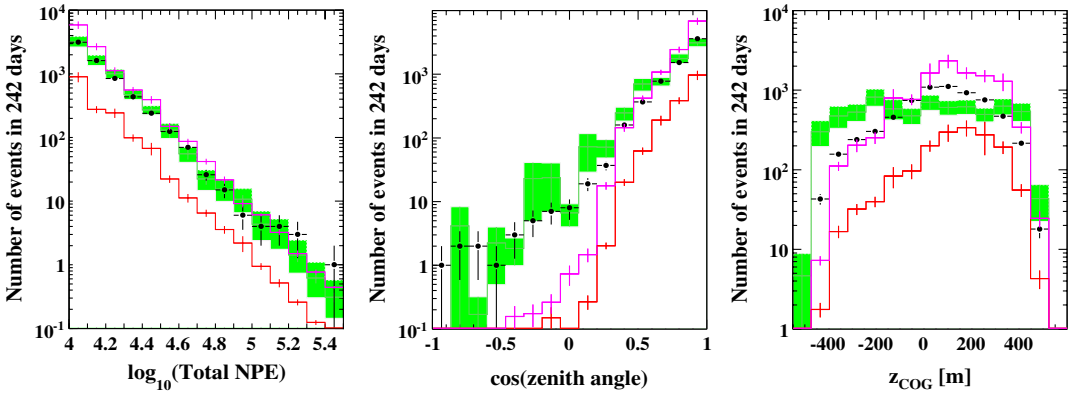

FIG. 2 (color online). Event distributions for NPE, cosine of reconstructed zenith angle, and the NPE-weighted mean depth of event (z_{COG}) for observational and the background Monte Carlo simulation data. The black dots represent observational data after the NPE $> 10^4$ cut, red for CORSIKA proton (SIBYLL), magenta for CORSIKA iron (SIBYLL). Green shaded regions represent distributions obtained with the empirical model with the size of shade expressing the uncertainty of the model. See text for the details.

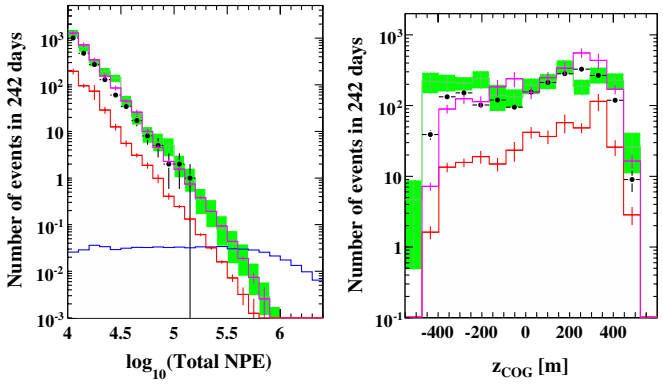

FIG. 3 (color online). Event distributions from the level-3 samples as functions of NPE (left) and z_{COG} (right). The black dots represent observational data, green boxes represent the empirical model including uncertainty. Red and magenta lines are CORSIKA samples with SIBYLL interaction model and proton and iron primaries, respectively. The left panel also includes the expected NPE distribution of events induced by the cosmogenic neutrinos [6] shown by the blue line for reference.

region (NPE $\geq 10^5$) is not used to avoid bias. The model provides a relation between the NPE of an event and the cosmic-ray primary energy. Its convolution with the cosmic-ray flux then gives the event rate with a given NPE. The cosmic-ray flux used in the present analysis is taken from the compilation in Ref. [2].

The model is based on the so-called Elbert formula [19] which parametrizes the mean multiplicity of muons with energies above a certain threshold E_μ:

$$N_\mu = \frac{E_T}{E_0}\frac{A^2}{\cos\theta'}\left(\frac{AE_\mu}{E_0}\right)^{-\alpha}\left(1-\frac{AE_\mu}{E_0}\right)^{\beta}, \quad E_T = 14.5\ \mathrm{GeV}, \tag{1}$$

where A, E_0, and θ' are the mass number, the energy, and the zenith angle of the primary cosmic ray [20]. The energy weighted integration of the formula relates the total energy carried by a muon-bundle E_μ^B to the primary cosmic-ray energy E_0,

$$E_\mu^B \equiv \int_\epsilon^{E_0/A}\frac{dN_\mu}{dE_\mu}E_\mu dE_\mu \simeq E_T\frac{A}{\cos\theta'}\frac{\alpha}{\alpha-1}\left(\frac{A\epsilon}{E_0}\right)^{-\alpha+1}, \tag{2}$$

assuming $AE_\mu/E_0 \ll 1$. Here, ϵ is empirically determined by fit to the observed data. Assuming its corresponding energy at the IceCube depth, $\epsilon^{\mathrm{in\text{-}ice}}$, is independent of zenith angle, ϵ (and thereby E_μ^B) can be calculated as a function of zenith angle by taking into account the energy loss during propagation through the Earth. The optimization of the two parameters α and $\epsilon^{\mathrm{in\text{-}ice}}$ is performed by comparing the observed data to simulation of a single high-energy muon with energy of E_μ^B in the NPE and zenith angle space, independently. $A = 1$ is assumed in the optimization. The event distributions derived from the empirical model with optimized parameters ($\alpha = 1.97$ and $\epsilon^{\mathrm{in\text{-}ice}} = 1500$ GeV) are given in Fig. 2. The green shaded region in the plot is obtained by allowing the model parameters to vary within $\pm 1\sigma$ from their optimized values.

The discrepancies of z_{COG} at large depths for the empirical model and at small depths for CORSIKA/iron seem to be due to vertical, down-going events because a restriction of the zenith angle, $\cos\theta < 0.8$, improves the agreement in both cases. Since the majority of the EHE neutrino induced events is close to the horizon we can discard all events with $\cos\theta < 0.8$ without significant loss of signal efficiency (level-3 cut). The resulting distributions are shown in Fig. 3.

C. Search for EHE cosmogenic neutrino signal

The level-4 cut to eliminate the muon background is carried out in the NPE-$\cos\theta$ (NZ) plane. In accordance with the requirements of blindness, the cuts are finalized on simulated events alone without referring to real data. Because the optical properties of the glacial ice vary significantly with depth [21], and because the changing absorption and scattering lengths affect what IceCube observes, the final cuts are chosen to be depth dependent. The cuts are chosen based on the depth of the weighted center of gravity of the event, z_{COG}. The distribution of events in the NZ plane depends on z_{COG}. We divide the events into two groups according to their z_{COG} as follows:

$$\text{region A: } -250 < z_{\mathrm{COG}} < -50\ \mathrm{m} \quad \text{and} \quad z_{\mathrm{COG}} > 50\ \mathrm{m},$$

$$\text{region B: } z_{\mathrm{COG}} < -250\ \mathrm{m} \quad \text{and} \quad -50 < z_{\mathrm{COG}} < 50\ \mathrm{m}.$$

As seen in Fig. 4, region B contains a large number of horizontal and up-going mis-reconstructed background events, whereas the fraction of such events in region A is

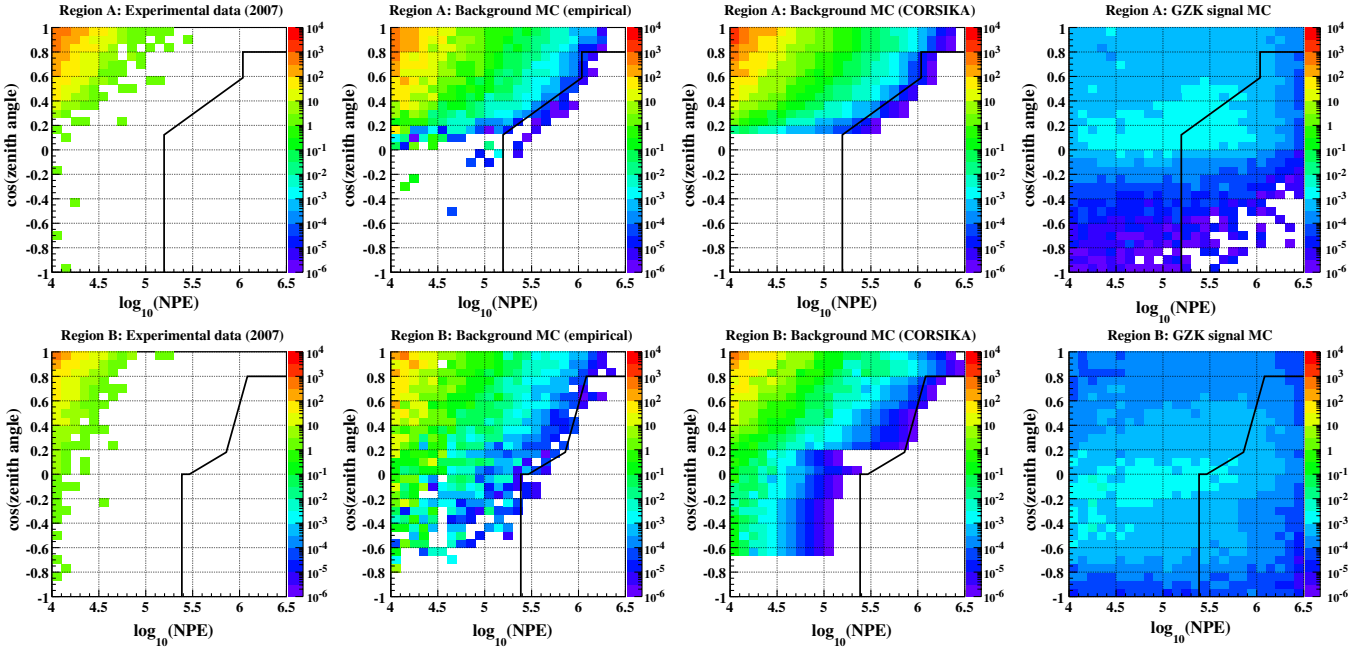

FIG. 4 (color online). Event number distributions passing the level-2 selection cut (NPE $> 10^4$) of the experimental data (left), the background from the empirical model (middle left), the background from CORSIKA-SIBYLL with iron primaries (middle right), and the signal (right) on the NZ plane at the IceCube depth. The upper (lower) panels show the distributions in the region A (B). The GZK neutrino flux [6] determines the event intensity in the signal Monte Carlo plot, adding all three flavors of neutrinos. The series of thick lines in each panel indicates the level-3 ($\cos(\theta) < 0.8$) and the final level-4 cuts.

very small. Figure 4 also shows the distributions of the experimental data and the simulated GZK neutrino induced signal events. The latter clearly accumulate near the horizontal direction regardless of the z_{COG} position and have on average larger NPE than the background sample. The selection criteria to separate signal from background are determined for region A and region B separately: For each bin of $\cos\theta$ (width 0.1), a threshold NPE is set such that the number of background events above the threshold is less than 10^{-4}. Tighter cuts to further reduce the background would also reduce the signal to an undesirable degree. The NPE thresholds in all the zenith angle bins are then connected to each other to form a series of lines on the NZ plane, defining the final level-4 cut, as drawn in Fig. 4. The cuts were optimized using the empirical model for background simulations, so we used extrapolated CORSIKA/iron data as a check of the final background level. Figure 4 also shows the distribution of background events in the NZ plane from the extrapolation. Table II summarizes the number of events remaining in the analysis after each of the cut levels.

The effective area as a function of energy at Earth's surface for each neutrino flavor is shown in the left panel of Fig. 5, averaged over all solid angles. The area increases with the energy owing to the increasing neutrino interaction cross sections and the increased probability of observing the interactions, which is different for each flavor.

At low energies, most of the ν_τ signal comes from events where the ν_τ interacts in the detector, or the τ decays in it. At higher energies, τ energy loss becomes large enough that through-going taus also pass the cuts. Contributions from ν_μ and ν_τ dominate over ν_e in the energy range above $\sim 10^8$ GeV, as the secondary produced muons and taus can travel long distances to reach the detection volume. This trend is reversed at lower energy where tau and muon energy losses are smaller, and ν_e's can deposit all of their energy into the detector volume. The effective area

TABLE II. Number of events at analysis filter levels for 242.1 days in 2007. The simulation predictions for the atmospheric muon background using the CORSIKA-SIBYLL package, the empirical model, and that for the GZK cosmogenic neutrino model are also listed for comparison. Errors shown here are statistical only. See Secs. IV B and IV C for details.

Analysis filter levels	Observational data	Empirical model	CORSIKA (iron)	CORSIKA (proton)	Signal (GZK1 [6])
Level 3 ($\cos(\theta) < 0.8$)	2014	$(2.65 \pm 0.21) \times 10^3$	$(2.68 \pm 0.19) \times 10^3$	$(4.16 \pm 0.40) \times 10^2$	$(620 \pm 7.3) \times 10^{-3}$
Level 4 (EHE ν search)	0	$(6.32 \pm 1.37) \times 10^{-4}$	$(4.18 \pm 1.29) \times 10^{-4}$	$(1.44 \pm 0.58) \times 10^{-4}$	$(155 \pm 1.4) \times 10^{-3}$

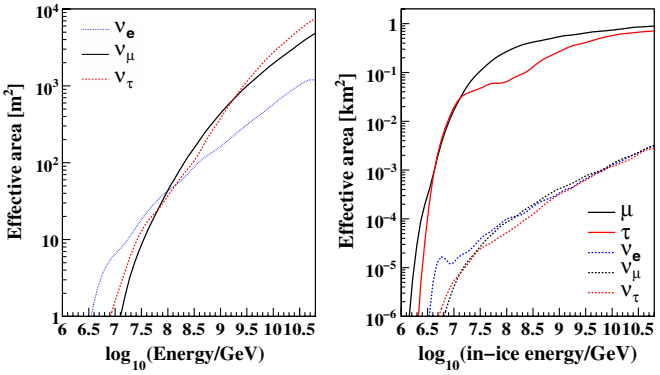

FIG. 5 (color online). The effective area of IC-22 for EHE neutrino search. The left panel shows the 4π solid angle averaged area as a function of neutrino energy at the Earth surface. The right panel shows the corresponding effective area for particles at 880 m from the IceCube center entering into the IC-22 fiducial volume. Muons and taus in this plot are secondary particles produced by neutrinos before reaching the neighborhood of the detector array. The energy here are defined as in-ice energy.

for ν_τ is larger than that for ν_μ at low energies, because of the events where taus decay inside the detector. At the highest energies, because of the larger mass of taus and increase of the tau decay time with energy, the tau range is longer than that of muons, leading to a larger effective area.

The right panel in Fig. 5 shows the effective area as a function of the in-ice energy (''in-ice area''). It represents the probability of detection of incoming particles with the present analysis. The area for incident muons and taus gradually increases with energy but is limited essentially by the physical cross section of the IC-22 array, $\sim$0.5 km^2. Because the Cherenkov yield of taus is smaller than muons with the same energy due to the smaller radiative energy loss, the detection probability of incident taus is lower, leading to the smaller in-ice area. Incoming neutrinos must interact to yield Cherenkov light to be detected. Therefore, the neutrino effective area becomes much smaller than that for muons or taus.

TABLE III. Expected event numbers passing the final level-4 selection criteria in the 2007 IC-22 observation. Models include the GZK models [6,22,23] and the *Z*-burst model [24]. The predictions are normalized to a live time of 242.1 days. Signal event numbers represent the sum over all three neutrino flavors. The first uncertainty is the statistical uncertainty determined by signal simulation statistics, and the second is the total systematic uncertainty from sources discussed in Sec. V.

Models	Number of Events per 242.1 days
GZK1 [6]	$(155 \pm 1.4^{+24}_{-40}) \times 10^{-3}$
GZK2 [22]	$(248 \pm 2.3^{+39}_{+65}) \times 10^{-3}$
GZK3 [23]	$(83 \pm 0.8 + ^{+13}_{-21}) \times 10^{-3}$
Z-burst [24]	$(398 \pm 3.4^{+63}_{-95}) \times 10^{-3}$

The expected number of signal events for various neutrino production models after the level-4 cut are summarized in TABLE III. GZK1 [6] represents the case of a moderately strong source evolution, $(z+1)^m$ with $m=4$ extending to $z=4.0$, while GZK2 [22] assumes $m=5$ up to $z=2.0$, and GZK3 [23] uses $m=3$ with a slightly different parametrization and a cutoff structure.

V. THE SYSTEMATICS

This search is based on the eventwise NPE and reconstructed zenith angle. The main systematic uncertainties derive from (1) the necessity to extrapolate the empirical fit to data by approximately an order of magnitude in NPE to estimate the background rate at the highest energies and from (2) the uncertainty of the absolute NPE scale. Table IV lists the sources of statistical and systematics errors.

A. Uncertainties in the background rate estimation

The largest uncertainty in the background rate estimate arises from the fact that the parameters of the empirical model were optimized for the observed events with $10^4 <$ NPE $< 10^5$ after level 2 selection. The limited statistics of this sample results in uncertainties on the parameters. The model was then extrapolated to a higher NPE region for the determination of the level-4 cut.

Allowing the parameters to vary within $\pm 1\sigma$ changes the background rate by between -59% (for the softest possible NPE spectrum after the level-4 cuts) and $+99\%$ (for the hardest possible NPE spectrum). Uncertainties in the detector sensitivity are incorporated by the parametrization. The difference in the background level estimated with the extrapolated CORSIKA/iron and the empirical model can be taken to indicate the level of systematic uncertainty due to model dependence. This uncertainty is approximately $\pm 15\%$ and can be assumed to include the possible contribution from charm decay. An uncertainty associated with the high-energy hadronic interaction model is evaluated using simulated muon-bundle intensity from SIBYLL and QGSJET-II with iron primaries and found to be $\pm 4\%$, which is negligible. An additional uncertainty of $\sim 17\%$ arises from the seasonal variation of the atmospheric muon rate as the signal selection criteria are based upon the season-averaged data.

B. Uncertainties of the signal rate estimate

The uncertainty in the relationship between measured NPE and the energies of charged particles is the largest systematic error affecting the signal event rate. It is the consequence of our limited understanding of the detector sensitivity, the photon propagation in ice, and the detector response to bright signals. It is evaluated using absolutely calibrated *in situ* light sources and amounts to a possible overestimation of NPE in simulation by 18.5%, which leads to decrease of the GZK signal rate by $\sim 21\%$.

TABLE IV. List of the statistical and systematic errors. The signal rate is estimated by assuming the high evolution flux $(m, Z_{max}) = (4, 4)$ in Ref [6].

Error source	Background rate	Signal (GZK) rate
Statistical error	$\pm 22\%$	$\pm 0.9\%$
Detector sensitivity	...	$\pm 8\%$
Yearly variation	$\pm 17\%$	...
Empirical model	$+99/-59\%$	...
Background model dep.	$\pm 15\%$	...
NPE yield	...	$+0/-21\%$
Neutrino cross section	...	$\pm 9\%$
Photonuclear interaction	...	$+10\%$
LPM effect	...	$\pm 1\%$
Total	$\pm 22\%$ (stat.)	$\pm 0.9\%$ (stat.)
	$+102/-63\%$ (sys.)	$+16/-26\%$ (sys.)

Uncertainties of the relevant particle interactions in the EHE regime also add systematics in the signal rate estimation. The expected event rate scales nearly linearly with the neutrino-nucleon inelastic cross section in the EHE range. This scaling has been confirmed by numerical studies, artificially increasing the cross section. The cross section uncertainty has been recently reduced to be around $\pm 9\%$ with the inclusion of the most recent data from HERA and modern parton distribution functions [25]. Another systematic error arises from the photonuclear cross section of EHE muons and taus. The present calculation used the model by Bugaev and Shlepin [26], rewritten in Ref. [27], that includes a relatively reliable soft nonperturbative component and a less certain hard perturbative part. Ignoring the hard component in the simulation gives the most conservative estimate of the uncertainty and leads to a 10% event rate increase. The suppression of bremsstrahlung and pair production due to the LPM effect [28], for the relevant electron energies of 10^{9-10} GeV, increases the effective radiation length of the electromagnetic cascade to $O(30\text{–}100)$ m from ~ 36 cm [29]. Because the value is still comparable to the IceCube DOM separation, and the contribution from ν_e constitutes $\leq 20\%$ of the total event rate in this energy range, the LPM effect has a negligible impact on the event rate. This has been confirmed by a special simulation study on ν_e including the LPM cascade elongation.

VI. RESULTS

No events are observed in the final data sample taken in 2007 with a live time of 242.1 days when applying the final level-4 selection criteria, which is consistent with the expected number of background events of 6.3×10^{-4}. We choose to present the resulting all flavor EHE neutrino upper limit in the quasi-differential form independent of the neutrino production model. Assuming full mixing due to oscillations, the experimental 90% confidence level upper limit is obtained by setting 2.44 events [30] for an upper bound of the number of events observed with bin width of a decade of energy with condition that energy dependence of neutrino flux multiplied by the effective area behaves as $\sim 1/E$ [31]. This limit is presented in Fig. 6 including the systematic errors. The plot indicates that the EHE neutrino search by the IceCube observatory is most sensitive to the neutrinos with energies on Earth's surface ranging between about 10^8 and 10^9 GeV. The absence of signal events in the sample of 242.1 days of effective live time results in a 90% C.L. differential upper limit on the neutrino flux of $E^2\phi_{\nu_e+\nu_\mu+\nu_\tau} \simeq 1.4 \times 10^{-6}$ GeV cm^{-2} sec^{-1} sr^{-1} on average for neutrinos with

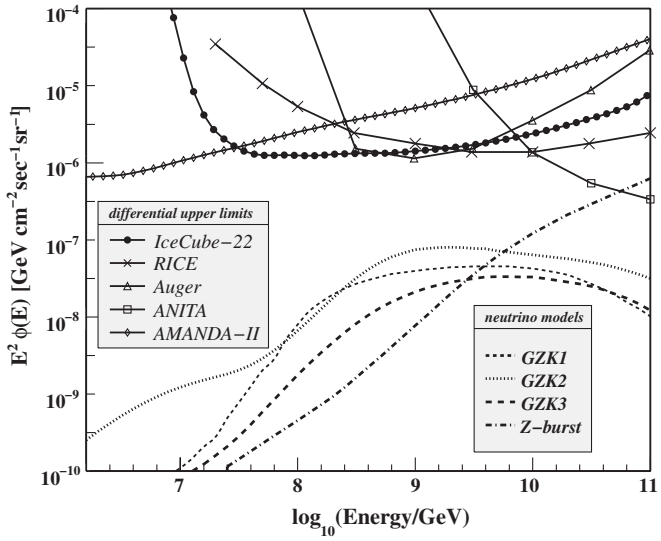

FIG. 6. The all flavor neutrino flux differential limit from the IC-22 EHE analysis (filled circles). The systematic errors are included. Also the various model predictions are shown for comparison: GZK model 1 [6] (short dashed line), GZK model 2 [22] (dotted line), GZK model 3 [23] (long dashed line), Z-burst model [24] (dashed dot line). The model independent differential upper limits by other experiments are also shown for Auger [32] (open triangles), RICE [31] (crosses), ANITA [34] (open squares), AMANDA [35] (rhombi). Limits from other experiments are converted to the all flavor limit assuming full mixing neutrino oscillations and 90% C.L when necessary.

an energy of $3 \times 10^7 \leq E \leq 3 \times 10^9$ GeV. Here $\phi_{\nu_e+\nu_\mu+\nu_\tau}$ denotes the differential flux of the sum over all three neutrino flavors, i.e. number of neutrinos per unit energy, area, time and solid angle.

The quasi-differential limit in Fig. 6 takes into account the systematic uncertainties. The background rate stays negligible $O(10^{-3})$ even including the systematic uncertainty and the resultant upper limit is unchanged. The signal rate uncertainty is strongly dominated by the uncertainty of the NPE yield which influences the number of expected signal events as a function of the neutrino energy. The upper limit is calculated by reducing NPE by 18.5% in the signal simulation to account for this factor. All the other sources of systematic error only slightly change the signal passing rate; they are independent of energy. They are included in the analysis by uniformly scaling the effective area in the limit calculation.

The present limit is approximately a factor of 20–30 higher than the intensity range expected in the GZK cosmogenic neutrino production models [6,22,23], as one can see in Fig. 6. The current limit for 242.1 days of observation is comparable to the Auger [32] and HiRes [33] bounds by their multiple year operation.

VII. CONCLUSIONS

The present work has demonstrated that the IceCube neutrino observatory is capable of searching for signatures of EHE cosmogenic neutrinos with relatively straightforward event selection methods. The model independent differential upper limit obtained with 242.1 days of observation in 2007, with approximately one quarter of the completed detector is $E^2\phi_{\nu_e+\nu_\mu+\nu_\tau} \simeq 1.4 \times 10^{-6}\,\mathrm{GeV\,cm^{-2}\,sec^{-1}\,sr^{-1}}$ for neutrinos with an energy of $3 \times 10^7 \leq E \leq 3 \times 10^9$ GeV. This is approximately a factor of 20 higher than the predicted GZK neutrino flux from relatively strongly evolved sources. In the future, data taken by IceCube with 40 to 86 strings operating should lead to a detection of cosmogenic neutrinos or a greatly improved limit.

ACKNOWLEDGMENTS

We acknowledge the support from the following agencies: U.S. National Science Foundation - Office of Polar Programs, U.S. National Science Foundation - Physics Division, University of Wisconsin Alumni Research Foundation, U.S. Department of Energy, and National Energy Research Scientific Computing Center, the Louisiana Optical Network Initiative (LONI) grid computing resources; Swedish Research Council, Swedish Polar Research Secretariat, Swedish National Infrastructure for Computing (SNIC), and Knut and Alice Wallenberg Foundation, Sweden; German Ministry for Education and Research (BMBF), Deutsche Forschungsgemeinschaft (DFG), Research Department of Plasmas with Complex Interactions (Bochum), Germany; Fund for Scientific Research (FNRS-FWO), FWO Odysseus programme, Flanders Institute to encourage scientific and technological research in industry (IWT), Belgian Federal Science Policy Office (Belspo); University of Oxford, United Kingdom; Marsden Fund, New Zealand; Japan Society for Promotion of Science (JSPS); the Swiss National Science Foundation (SNSF), Switzerland. A. Kappes and A. Groß acknowledge support by the EU Marie Curie OIF Program. J. P. Rodrigues acknowledges support by the Capes Foundation, Ministry of Education of Brazil. This analysis work has been particularly supported by the Japan-US Bilateral Joint Projects in the Japan Society for the Promotion of Science.

[1] For a review, see, e.g. J. W. Cronin, Rev. Mod. Phys. **71**, S165 (1999); S. Yoshida and H. Dai, J. Phys. G **24**, 905 (1998).
[2] M. Nagano and A. A. Watson, Rev. Mod. Phys. **72**, 689 (2000).
[3] N. Hayashida *et al.*, Phys. Rev. Lett. **77**, 1000 (1996); J. Abraham *et al.* (Pierre Auger Collaboration), Science **318**, 938 (2007).
[4] K. Greisen, Phys. Rev. Lett. **16**, 748 (1966); G. T. Zatsepin and V. A. Kuzmin, Pis'ma Zh. Eksp. Teor. Fiz. **4**, 114 (1966) [JETP Lett. **4**, 78 (1966)].
[5] V. S. Berezinsky and G. T. Zatsepin, Phys. Lett. **28B**, 423 (1969).
[6] S. Yoshida and M. Teshima, Prog. Theor. Phys. **89**, 833 (1993).
[7] A. Achterberg *et al.* (IceCube Collaboration), Astropart. Phys. **26**, 155 (2006).
[8] F. Halzen and D. Hooper, Phys. Rev. Lett. **97**, 071101 (2006).
[9] S. Yoshida *et al.*, Phys. Rev. D **69**, 103004 (2004).
[10] R. Abbasi *et al.* (IceCube Collaboration), Nucl. Instrum. Methods Phys. Res., Sect. A **601**, 294 (2009).
[11] R. Abbasi *et al.* (IceCube Collaboration), Astrophys. J. Lett. **689**, L65 (2008).
[12] R. Abbasi *et al.* (IceCube Collaboration), Nucl. Instrum. Methods Phys. Res., Sect. A **618**, 139 (2010).
[13] J. Jones, I. Mocioiu, M. H. Reno, and I. Sarcevic, Phys. Rev. D **69**, 033004 (2004).
[14] D. Heck *et al.*, Forschungszentrum Karlsruhe Report No. FZKA 6019 (1998).
[15] T. S. Sinegovskaya and S. I. Sinegovsky, Phys. Rev. D **63**, 096004 (2001).
[16] R. Enberg, M. H. Reno, and I. Sarcevic, Phys. Rev. D **78**, 043005 (2008).

[17] D. Chirkin and W. Rhode, arXiv:hep-ph/0407075v2.
[18] J. Lundberg *et al.*, Nucl. Instrum. Methods Phys. Res., Sect. A **581**, 619 (2007).
[19] T. K. Gaisser, *Cosmic Rays and Particle Physics* (Cambridge University Press, Cambridge, England, 1990), p. 206.
[20] J. W. Elbert, in *Proceedings of the DUMAND Summer Workshop, La Jolla, California, 1978*, edited by A. Roberts (Scripps Institution of Oceanography, La Jolla, CA, 1979) Vol. 2, p. 101.
[21] M. Ackermann *et al.*, J. Geophys. Res. **111**, D13203 (2006).
[22] O. E. Kalashev, V. A. Kuzmin, D. V. Semikoz, and G. Sigl, Phys. Rev. D **66**, 063004 (2002).
[23] R. Engel, D. Seckel, and T. Stanev, Phys. Rev. D **64**, 093010 (2001).
[24] S. Yoshida, G. Sigl, and S. Lee, Phys. Rev. Lett. **81**, 5505 (1998).
[25] A. Cooper-Sarkar and S. Sarkar, J. High Energy Phys. 01 (2008) 075.
[26] E. V. Bugaev and Yu. V. Shlepin, Phys. Rev. D **67**, 034027 (2003).
[27] E. Bugaev, T. Montaruli, Y. Shlepin, and I. Sokalski, Astropart. Phys. **21**, 491 (2004).
[28] L. Landau and I. Pomeranchuk, Dokl. Akad. Nauk SSSR **92**, 535 (1953); A. Migdal, JETP **5**, 527 (1953).
[29] S. Klein, Rev. Mod. Phys. **71**, 1501 (1999).
[30] G. J. Feldman and R. D. Cousins, Phys. Rev. D **57**, 3873 (1998).
[31] I. Kravchenko *et al.* (Rice Collaboration), Phys. Rev. D **73**, 082002 (2006).
[32] J. Abraham *et al.* (Pierre Auger Collaboration), Phys. Rev. D **79**, 102001 (2009).
[33] R. U. Abbasi *et al.* (HiRes Collaboration), Astrophys. J. **684**, 790 (2008).
[34] P. W. Gorham *et al.* (ANITA Collaboration), Phys. Rev. D **82**, 022004 (2010).
[35] M. Ackermann *et al.* (IceCube Collaboration), Astrophys. J. **675**, 1014 (2008).